Submitted to JPCA, 8/9/2022, revised 9/2/2022

Nonadiabatic Reactive Quenching of OH($A^2\Pi^+$) by H_2: Origin of High Vibrational Excitation in the H_2O Product

Shanyu Han,[1] Bin Zhao,[2] Riccardo Conte,[3] Christopher L. Malbon,[4,%] Joel M. Bowman,[5] David R. Yarkony,[4] Hua Guo[1,*]

[1]*Department of Chemistry and Chemical Biology, University of New Mexico, Albuquerque, NM 87131, USA*

[2]*School of Chemistry, Southern University of Science and Technology, Shenzhen, 518055, China*

[3]*Dipartimento di Chimica, Università degli Studi di Milano, via Golgi 19, 20133 Milano, Italy*

[4]*Department of Chemistry, Johns Hopkins University, Baltimore, Maryland 21218, USA*

[5]*Department of Chemistry and Cherry L. Emerson Center for Scientific Computation, Emory University, Atlanta, Georgia 30322, USA*

*: corresponding author, hguo@unm.edu

%: present address: Department of Chemistry, Yale University, New Haven, CT 06520

Abstract

The nonadiabatic dynamics of the reactive quenching channel of the OH $\left(A^2\Sigma_g^+\right)$ + H_2/D_2 collisions is investigated with a semi-classical surface hopping method, using a recently developed four-state diabatic potential energy matrix (DPEM). In agreement with experimental observations, the H_2O/HOD products are found to have significant vibrational excitation. Using a gaussian binning method, the H_2O vibrational state distribution is determined. The preferential energy disposal into the product vibrational modes is rationalized by an extended Sudden Vector Projection model, in which the **h** and **g** vectors associated with the conical intersection are found to have large projections with the product normal modes. However, our calculations did not find significant insertion trajectories, suggesting the need for further improvement of the DPEM.

TOC graphic

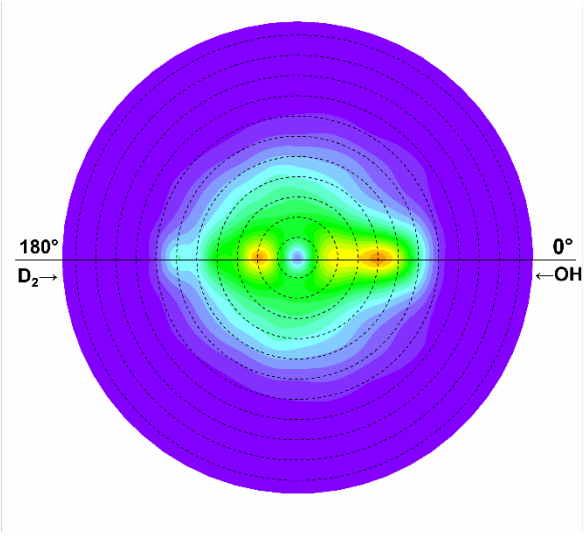

I. Introduction

The hydroxyl radical (OH) is an important oxidizing agent in combustion[1] and Earth's atmosphere.[2] Laser induced fluorescence (LIF) via $OH(A^2\Sigma_g^+)$ has been widely used in kinetic diagnostics.[3] In gaseous environments, however, the excited $OH(A^2\Sigma_g^+)$ radical can also be efficiently quenched by collisions with other gas molecules, thus affecting the LIF.[4] Consequently, an in-depth understanding of the radiationless decay is needed. It is now well established that the electronic quenching proceeds via a nonadiabatic mechanism facilitated by conical intersections (CIs).[5] Indeed, the nonadiabatic quenching of $OH(A^2\Sigma_g^+)$ radicals through collisions with H_2 has served as a benchmark system for understanding nonadiabatic dynamics of bimolecular collisions.

The quenching of $OH(A^2\Sigma_g^+)$ by H_2 can proceed through either a nonreactive channel:

$$OH(A^2\Sigma_g^+) + H_2(X^1\Sigma_g^+) \rightarrow OH(X^2\Pi) + H_2(X^1\Sigma_g^+) \quad \text{(R1a)}$$

or a reactive channel:

$$OH(A^2\Sigma_g^+) + H_2(X^1\Sigma_g^+) \rightarrow H_2O(\tilde{X}^1A_1) + H \quad \text{(R1b)}$$

In addition, there also exists an adiabatic channel:

$$OH\left(A^2\Sigma_g^+\right) + H_2\left(X^1\Sigma_g^+\right) \rightarrow OH\left(A^2\Sigma_g^+\right) + H_2\left(X^1\Sigma_g^+\right) \quad \text{(R1c)}$$

consisting of elastic and inelastic scattering between the two molecules.

Lester and co-workers have extensively investigated this system,[6-12] in which OH $\left(A^2\Sigma_g^+\right)$ was prepared in its ground ro-vibrational state at a low temperature and allowed to collide with H_2 with an average collision energy of 0.025 eV. These authors identified both the nonreactive and reactive channels (R1a and R1b) and deduced from the measured R1a yield the latter (R1b) as the dominant one.[9] In the highly exothermic reactive quenching channel, the kinetic energy distribution of the H product measured from its Doppler profile was found to be bimodal, suggesting complex dynamics with at least two reaction pathways.[7, 9, 12] The major peak of the distribution lies below 0.5 eV, suggesting that the energy release of 4.83 eV is mainly disposed as the internal energy of the H_2O co-product. A subsequent crossed-beam experiment by Davis and coworkers on $OH\left(A^2\Sigma_g^+\right) + D_2\left(^1\Sigma_g^+\right)$ collisions at 0.16 eV of collision energy confirmed the large internal excitation of the HOD product,[13] although their kinetic energy distribution of D measured via Rydberg tagging was broader and has only a single peak. More recently, Brouard *et al.* reported a molecular beam investigation and found that the adiabatic channel (R1c) has a much larger cross section than the quenching channels (R1a and R1b).[14]

One of the interesting experimental findings by Lester and coworkers is the significant yield (~25 %) of the H_2O + D products from the H_2 + OD collision, along with the major HOD + H products (~75%).[12] The minor product was proposed to have formed from an insertion pathway, in which the OD inserts into the H-H bond, followed by decay of the H_2DO complex to the H_2O and D products. Similar observations were reported for the D_2 + OH collision.[7] This pathway might play a role in the fast component of the H kinetic energy distribution in the H_2 + OH collision, which was also found by the same group.[12] In the latter case, the insertion is not easily distinguished from the main abstraction channel because of the identical H nuclei.

Complementing the experimental studies mentioned above, theoretical investigations have provided much insight into the electronic structure of this prototypical system and the resulting dynamics.[8, 15-27] There are three states involved: the 1^2A, 2^2A, and 3^2A states, which have $^2A'$, $^2A''$ and $^2A'$ symmetries at planar geometries, respectively. Early ab initio studies identified a T-shaped (C_{2v}) CI between the 3^2A state (A_1 irreps at C_{2v} geometries) correlated to the OH $\left(A^2\Sigma_g^+\right)$ + H_2 asymptote and the lower 2^2A state (B_2 irreps at C_{2v} geometries), which is apparently responsible for nonadiabatic transitions leading to the quenching products.[15] A CI is a cone-shaped degeneracy between electronic adiabatic PESs and forms the gateway for nonadiabatic transitions.[28-30] Later studies found that the T-shaped (C_{2v}) and linear ($C_{\infty v}$) (3^2A, 2^2A) CIs are connected by a crossing seam with planar (C_s) geometrises.[16,

[17] Another CI between the 2^2A and 1^2A states was found to be part of another seam extending to non-planar geometries.[22, 23] Both CIs have a distinct orientation with OH pointing its O end to H_2. Interestingly, a Rydberg-like H_3O minimum was found on the 2^2A state PES,[22] which might be responsible for the insertion pathway found in the deuterated experiments.[7, 12] More recent studies reported reduced- and full-dimensional PESs in either the adiabatic or diabatic representations,[18-21, 25, 26] which enabled dynamics calculations yielding attributes that can be directly compared to the experiments.[18-21, 24, 27, 31]

Very recently, we reported a theoretical study on the collision dynamics between OH$\left(A^2\Sigma_g^+\right)$ and H_2 using a full-dimensional quantum model with zero total angular momentum.[31] The quantum dynamics calculation was based on a four-state diabatic potential energy matrix (DPEM) developed by Malbon, Zhao, Guo and Yarkony (MZGY).[26] For the nonreactive channel, the experimental OH(X^2-اا) rovibrational and Λ-doublet distributions were well reproduced. Most importantly, the results suggested a dominant adiabatic channel (R1c), consistent with the observations by Brouard and coworkers.[14] The large elastic and inelastic cross sections in the adiabatic channel R1c were attributed to the unique stereodynamics in this system. While nonadiabatic transitions to lower electronic states occur largely in the HO-HH orientation, leading to the collinear CIs,[31] collisions in the OH-HH orientation are mostly adiabatic.[31] The quantum dynamics calculations also found that the reactive and nonreactive quenching channels have branching fractions of the same order of magnitude,

consistent with another earlier trajectory surface hopping (TSH) calculations by Collins *et al.*[21] on a different DPEM, but different from the experimentally based estimate of Lester and coworkers.[9] With the inclusion of the (in)elastic channel, which was ignored in the earlier model,[9] the measured and calculated branching fractions of the three channels become consistent.[31] This conclusion was further confirmed by a more recent TSH study[27] using an improved DPEM developed independently by Shu *et al.*[25]

In contrast to the extensively investigated OH$(X^2\Pi)$ + H_2 channel, the H + H_2O channel received much less attention. The earlier TSH study by Collins *et al.*[21] reported angular and kinetic energy distributions of the products in R1b, but did not resolve the internal state distribution of the H_2O product. Neither did they explain why/how the large energy release is deposited among the internal modes of the H_2O(HOD) product. This question has been partially addressed by Bowman and coworkers,[20, 24] who revealed that the large energy release is almost exclusively into the vibrational modes with limited rotational excitation. However, that study started the trajectories near the CI seam on the ground state PES, thus did not include the initial collision dynamics and the subsequent nonadiabatic transitions. Nor did it explore the possible insertion channel.

In this work, we report a new and thorough theoretical investigation of R1, focusing on the R1b channel. Both the H_2 + OH and D_2 + OH processes are investigated. The dynamics is characterized on the MZGY DPEM[26] using a semi-classical TSH method. The vibrational distribution of the H_2O/HOD product is

resolved using the 1GB method, a modified Gaussian binning[32] method developed by Czako and Bowman.[33] In addition, we propose an extended version of the Sudden Vector Projection (SVP) model[34] to rationalize the energy disposal in the products. This nonadiabatic version of SVP is shown to explain energy disposal in products of both the reactive and non-reactive quenching channels. This work is organized as follows. Section II presents the method used in dynamics calculations and an extended version of the SVP model to analyze the mode-specificity in product energy disposal. The results and discussions are presented in Section III, and the final section concludes the paper.

II. Methods

IIA. Nonadiabatic Dynamics

The extensively tested[27, 31] 4-state MZGY DPEM, whose details can be found in a previous paper,[26] is used in the present work. The nonadiabatic dynamics of OH $\left(A^2\Sigma_g^+\right)$ +H_2/D_2 $\left(X^1\Sigma_g^+\right)$ collisions were investigated with fewest switches method with time uncertainty and stochastic decoherence (FSTU/SD),[35] as implemented in the Adiabatic and Non-adiabatic Trajectories (ANT) package.[36] This method adds time uncertainty[37] and stochastic decoherence[35] to the fewest-switches TSH method of Tully.[38] It has been used in our recent work on the non-reactive quenching channel and good agreement with quantum dynamics results was found.[27]

The initial atomic coordinates and momenta in the Cartesian coordinates were sampled from the rovibrational ground state of OH $\left(A^2\Sigma_g^+\right)$ and H_2/D_2 $\left(^1\Sigma_g^+\right)$ reactants using the harmonic oscillator and rigid rotor approximations. The coupling between the rotational quantum number and non-zero electronic spin of OH $\left(A^2\Sigma_g^+\right)$ is ignored. About 1,000,000 and 400,000 trajectories were propagated for the OH + H_2 and OH + D_2 collisions, respectively. The large number of trajectories in the former was needed to resolve the H_2O product vibrational states. The calculations were performed in the adiabatic representation with the collisional energy chosen at 0.16 eV(15.5 kJ/mol) in order to compare with the beam experiment of Ortiz-Suárez *et al.*[13] The impact parameter *b* was randomly sampled from a uniformly distributed random number $\zeta \in [0,1]$, according to $b = b_{\max}\sqrt{\zeta}$ with $b_{\max}$=5.5 Angstrom. A trajectory is terminated when the separation between the two products reaches 5 Å.

IIB. Gaussian binning (1GB) for product vibrational states

For each trajectory, the final Cartesian coordinates and velocities of an *N*-atom polyatomic product, denoted as $\mathbf{r}_i$ and $\mathbf{v}_i$ (*i*=1~*N*) need to be transformed to the center of mass frame for the following vibrational product analysis. The overall angular momentum is removed from the velocities by:

$$\mathbf{v}_i^{nr} = \mathbf{v}_i - \boldsymbol{\Omega} \times \mathbf{r}_i \text{ and } \boldsymbol{\Omega} = \mathbf{I}^{-1}\mathbf{j}, \quad (1)$$

where $\mathbf{I}^{-1}$ is the inverse of the moment of inertia tensor and $\mathbf{j} = \sum_{i=1}^{N} \mathbf{r}_i \times (m_i \mathbf{v}_i)$. Then, $\mathbf{r}_i$ and $\mathbf{v}_i^{nr}$ need to be rotated to the Eckart frame[39] corresponding to reference geometry $\mathbf{r}_i^{eq}$:

$$\mathbf{r}_i^{Ec} = \mathbf{C}\mathbf{r}_i \text{ and } \mathbf{v}_i^{nr,Ec} = \mathbf{C}\mathbf{v}_i^{nr}, \qquad (2)$$

in which more details about the transformation matrix $\mathbf{C}$ can be found in Ref. 40.

Normal-mode analysis of the product molecule was then performed. The harmonic frequencies $\omega_k (k = 3N - 6)$ of a non-linear molecule are obtained by diagonalizing the Hessian matrix at its equilibrium structure in the center of mass frame, which is denoted as $\mathbf{r}_i^{eq}$. The corresponding eigen vectors form the transformation matrix $\mathbf{L}$, which transform from mass-scaled Cartesian coordinates to normal mode coordinates Q_k and momenta P_k:

$$Q_k = \sum_{i=1}^{N} \sqrt{m_i}\mathbf{L}_{ki}\Delta\mathbf{r}_i, \quad k = 1, 2, \ldots, 3N - 6 \qquad (3a)$$

$$P_k = \sum_{i=1}^{N} \sqrt{m_i}\,\mathbf{L}_{ki}\,\mathbf{v}_i^{\mathrm{E.c,nr}} \qquad k = 1, 2, \ldots, 3N - 6,$$

(3b)

where $\Delta\mathbf{r}_i = \mathbf{r}_i^{\mathrm{E.c}} - \mathbf{r}_i^{\mathrm{eq}}$.

Thus, the classical harmonic energy and action for each normal mode are determined by:

$$E_k = \frac{P_k^2}{2} + \frac{1}{2}\omega_k^2 Q_k^2,$$

(4)

$$n_k = \frac{E_k}{\omega_k} - \frac{1}{2}, \quad k = 1, 2, \ldots, 3N - 6, \tag{5}$$

where E_k is the harmonic energy for *k*-th vibration mode. The integer vibrational quanta are assigned to quantum states by rounding to the nearest integer value *n*. The vibrational state with (n_1, n_2 , …, $n_{3N\text{-}6}$) as the collection of vibrational quantum numbers is denoted collectively as $\mathbf{n}$.

The vibrational quantum numbers determined by the aforementioned procedure is often called histogram binning (HB).[41] Bonnet has shown that it is generally better to bin the vibrational actions using Gaussian weight functions centered at the integers.[32] However, such a Gaussian binning (GB) method is too numerically expensive for polyatomic molecules. Czako and Bowman proposed a more efficient approach called 1GB, in which the binning is not performed for each vibrational mode, but for each

vibrational quantum state labeled by **n**.[33, 40] This approach was further improved by Conte and Bowman,[24] who replaced the harmonic energies in Eq. (4) with accurate energies of the vibrational levels of the molecule. This improvement is particular relevant to highly excited vibrational states where the anharmonicity is large. In this improved 1GB approach, the weight of the product from each trajectory is a single Gaussian of the difference between the classical vibrational energy $E(\mathbf{n}'_p)$ of the *p*-th trajectory and the energy of the corresponding vibrational state associated with quantum numbers **n** ($E(\mathbf{n})$):

$$G_p(\mathbf{n}') = \frac{\beta}{\sqrt{\pi}} e^{-\beta^2 \left[E(\mathbf{n}'_p) - E(\mathbf{n})\right]/2E(\mathbf{0})^2} \tag{6}$$

where $\beta = 2\left[\ln(2)\right]^{\frac{1}{2}}/\delta$, δ is the full-width at half maximum, and $E(\mathbf{0})$ is the zero point energy. The classical vibrational energy is calculated by:

$$E(\mathbf{n}'_p) = \frac{1}{2}\sum_{i=1}^{N} m_i \mathbf{v}_{i,p}^{nr} \left(\mathbf{v}_{i,p}^{nr}\right)^{\mathrm{T}} + V(\mathbf{r}_{1,p}, \mathbf{r}_{2,p}, ..., \mathbf{r}_{N,p}) - V(\mathbf{r}_{1,p}^{eq}, \mathbf{r}_{2,p}^{eq}, ..., \mathbf{r}_{N,p}^{eq}) \tag{7}$$

.

The vibrational energies $E(\mathbf{n})$ for H_2O used in this study were taken from Ref. 42, which was obtained using a quantum method on an accurate PES of H_2O. Such 1GB analysis was not performed for HOD because of the lack of assignment of the highly excited vibrational levels.

IIC. Sudden Vector Projection

In the original Sudden Vector Projection (SVP) model,[43] the ability of a reactant mode in promoting the reaction is given by the projection of the corresponding normal mode vector onto the reaction coordinate at the transition state. By microscopic reversibility, the SVP model can also be used to predict the energy disposal into different product modes. This model has been successfully applied to direct reactions with and without an activation barrier.[34]

Here we extend this idea to rationalize the product energy disposal in non-adiabatic reactions dominated by a CI. The basic premise is that the product energy disposal is dictated by the forces exerted on the system immediately after nonadiabatic transitions near the CI, which is in the same spirit as the recent work of Fu *et al.*[20] who sampled the trajectories near the crossing seam. Hence, the bottleneck is assumed to be the CI which is an N^{int}-2 dimensional seam (N^{int} is the number internal degrees of freedom). At the CI seam between the *I*th and *J*th electronic states, the degeneracy is lifted by two orthogonal vectors, namely the *g* and *h* vectors.[44] The *g* vector is defined as the derivative of the adiabatic energy difference:

$$2g_{IJ} = \nabla(E_I - E_J) \tag{8}$$

and *h* vector is approximately parallel to the derivative coupling f_{IJ} :

$$h_{IJ} \approx f_{IJ} \times (E_I - E_J) . \tag{9}$$

As the CI region is viewed as the bottleneck, we use the *g* and *h* vectors to predict the mode specificity in product energy disposal. In the current system, the non-adiabatic transitions occur predominantly at linear configuration,[31] the *g* and *h* vectors

are obtained at the lowest energy linear CI seam between the 2^2A and 1^2A states. The projections are denoted as $Q(v)\cdot g$ and $Q(v)\cdot h$, where $Q(v)$ is a product normal mode vector, taken as the column vector of $\mathbf{L}$ for vibrational mode *v*. For the translational vector $Q(trans)$, it is defined by allowing an infinitesimal displacement along the scattering coordinate without inducing a movement in the center of mass frame. In practice, the orientation of the coordinate system of the product molecule contains some arbitrariness. So, the coordinate frame of the product H_2O is transformed to the Eckart frame corresponding to reference geometry that is chosen to be the CI geometry.

III. Results

At least three adiabatic states are needed to understand the quenching of OH $\left(A^2\Sigma_g^+\right)$ by H_2. The highest adiabat, 3^2A, is correlated with the reactant asymptote, while the lower two adiabats, 2^2A and 1^2A, form the degenerate pair of the OH $\left(X^2\Pi\right)$ + H_2 asymptote of R1a. The H_2O + H asymptote of R1b is correlated with the 1^2A state. There are two CI seams between the three states,[22, 23] leading to nonadiabatic transitions from the 3^2A and 2^2A states followed by those from the 2^2A to 1^2A states. Previous dynamics calculations have shown that such transitions occur mostly near

the linear ($C_{\infty v}$) geometry.[27, 31] In Figure 1a, the adiabatic PESs of the three states at collinear HO-HH geometry and their correlations to various asymptotes are shown.

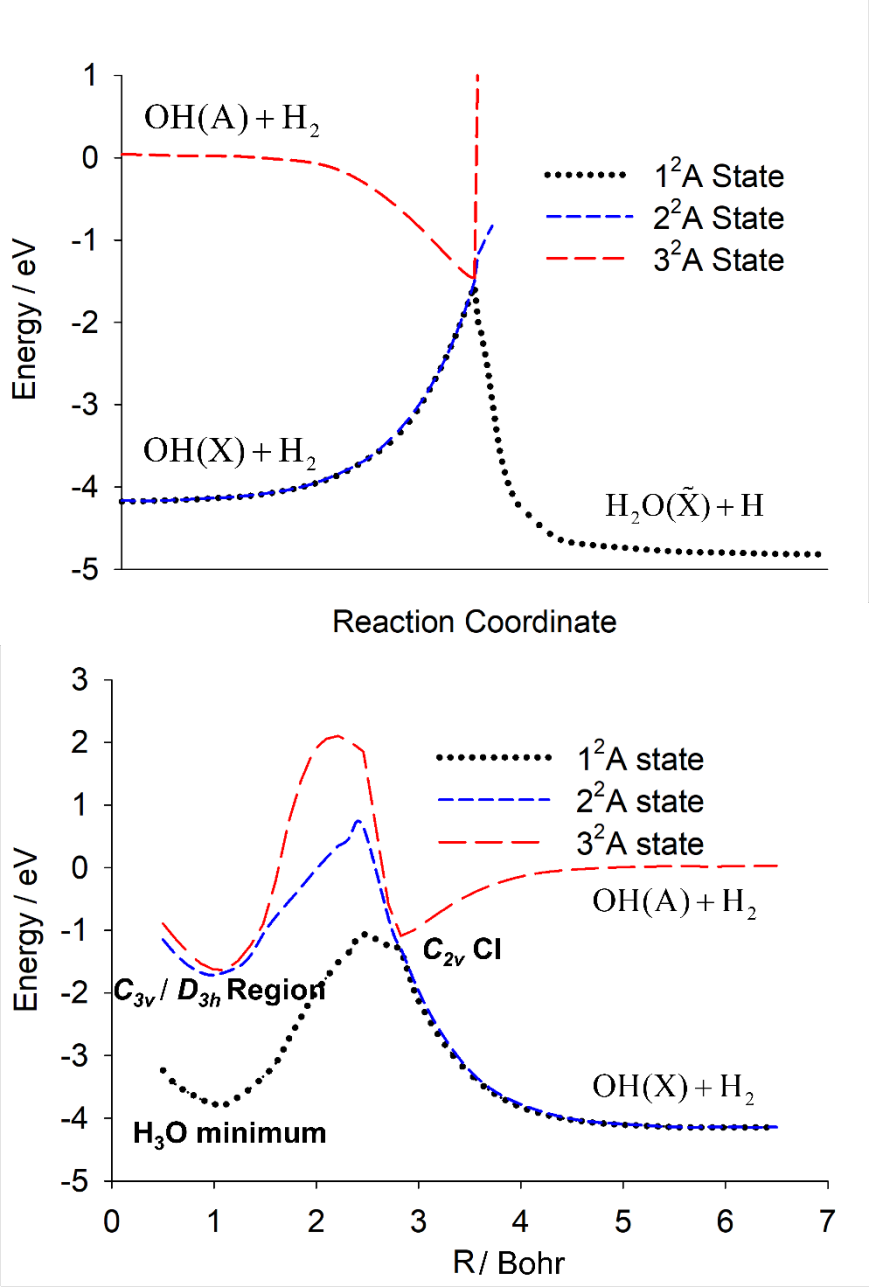

Figure 1. (Upper panel) potential energy surfaces involved in OH(A) + H_2 scattering, including both the reactive and non-reactive quenching channels via the $C_{\infty v}$ conical

intersections. (Lower panel) PESs of the insertion pathway as function of *R*, generated with the C_{2v} geometric restriction (θ_{OH} and θ_{H_2} are fixed at 0 and 90°) by optimizing the bond lengths of r_{OH}, r_{H_2} and φ with respect the adiabatic energy of the 3^2A state. The coordinate system is defined in Figure 2.

For the OH$\left(A^2\Sigma_g^+\right)$ collision with H_2, about 9000 out of a total of 1,000,000 trajectories were found in reactive quenching channel, yielding a branching ratio of ~1 % which is consistent with the previous report.[27] For the OH$\left(A^2\Sigma_g^+\right)$ + D_2 scattering, about 4000 trajectories were found in the HOD + D product channel from 400,000 trajectories, yielding roughly the same branching fraction. The small branching ratio of the R1b channel required a very large number of trajectories to achieve reasonable statistics, especially if the product vibrational distribution is to be resolved.

In our previous study of the nonreactive quenching channel, we have discussed its stereodynamics,[31] namely the dependence on the orientation of the collision partners. The anisotropy of the 3^2A PES is such that non-adiabatic transitions are near the HO-HH (HO-DD) linear CIs in the nonreactive quenching channel.[31] A natural question is whether nonadiabatic transitions in the reactive quenching channel exhibits a similar tendency. As confirmed in Figure 2, the geometries of the hopping positions are

mostly located near the linear CIs, implying that both the R1a and R1b channels have the same nonadiabatic origin, despite the fact that the two diverge after the initial transition, as illustrated in the upper panel of Figure 1. The observed propensity for nonadiabatic transitions occurring near linearity suggest that the adiabatic model in Ref. 20 might not have the correct weight concerning the initial conditions since it assumed equal probability for nonadiabatic transitions at different CI seam geometries, including those with linear (C_s) and T-shaped (C_{2v}) geometries.

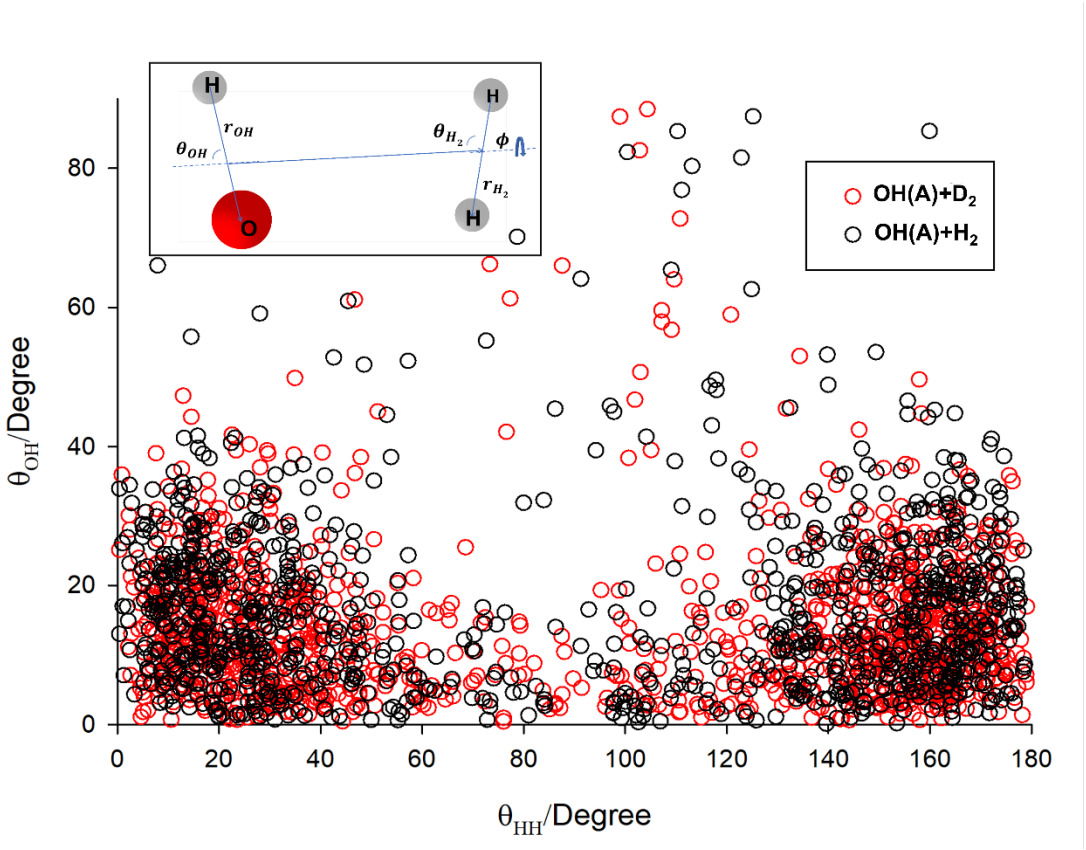

Figure 2. Distribution of the diatomic polar angles (defined in the *Inset*) at the 3^2A-2^2A transitions for the reactive quenching channel. Red and black circles represent OH(A) + H_2 and OH(A) + D_2 processes, respectively.

Figure 3 presents the distribution of the center-of-mass scattering angle (θ) from the TSH simulation of the OH(A) + D_2 → HOD + D reaction at the collision energy of 0.16 eV. The experimental differential cross section (DCS) of Ortiz-Suárez *et al*.[13] and the previous theoretical distribution of Collins *et al*.[21] are included in the same figure for comparison. The agreement of our results with experiment is satisfactory, confirming the accuracy of the DPEM as well the dynamics simulation. The agreement between the two theoretical DCSs is also quite reasonable, suggesting similar non-adiabatic dynamics.

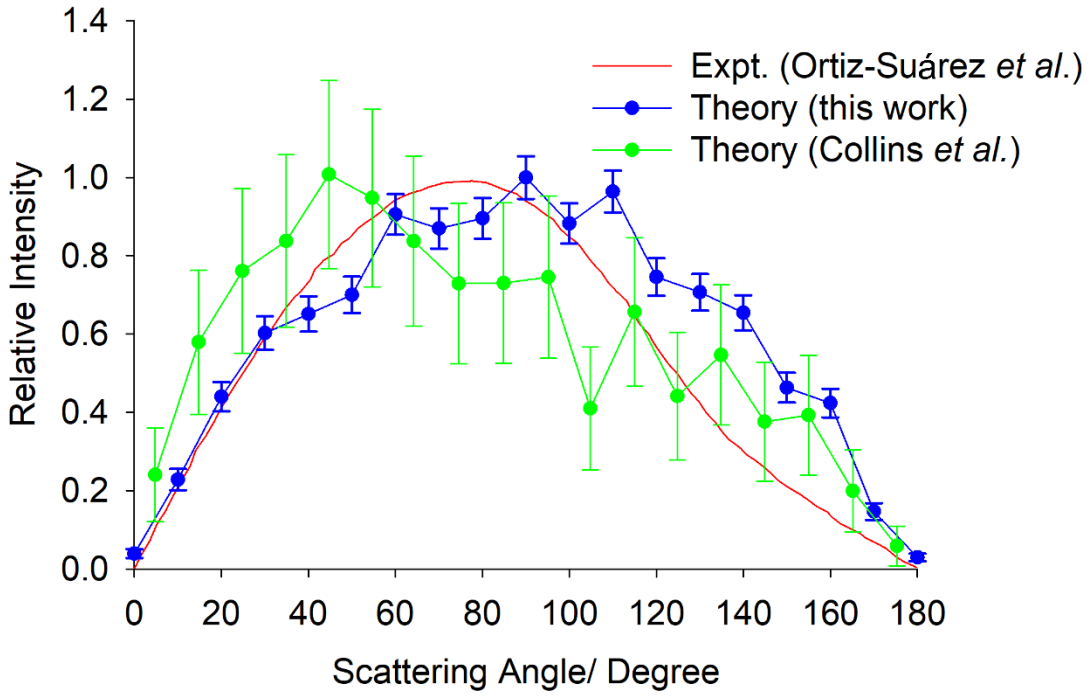

Figure 3. Comparison of the calculated product angular distribution of D_2 + OH(A) → HOD + D to the experimental[13] and previous theoretical results.[21] The scattering angle is defined such that forward scattering corresponds to the scattered D atom is aligned

with the initial direction of D_2. The experimental data have been multiplied by $\sin(\theta)$ for comparison. The statistic errors are given by the error bars for the theoretical results.

In the experimental DCS, two decomposition schemes were proposed for the kinetic energy and angular distributions.[13] One decomposition called for the major channel with forward scattering and the minor backward scattering channel. Alternatively, the DCS is fit with a major forward scattering channel and a minor forward-backward scattering, which implies long-lived intermediate complex. Such decomposition is empirical because of the lack of knowledge of the correlation between the two distributions. To gain insights into the reaction mechanism, the lifetime distributions are displayed in Figure 4, in which the lifetime of a trajectory is defined by the time difference (T_i-T_f). T_i is defined as the time when the distance between the mass centers between OH and H_2 reaches 3.5 Bohr, and T_f is defined as the time when the H_2 bond length reaches 3.0 Bohr. Based on the lifetime distribution, we can conclude that the abstraction is a direct process without obvious long-lived intermediate complex. This is confirmed by the correlation between the impact parameter and scattering angle, as shown in Figure 5. From this figure, it is clear that the scattering angle is inversely proportional to the impact parameter. A small impact parameter leads to backward scattering while a large impact parameter to forward scattering.

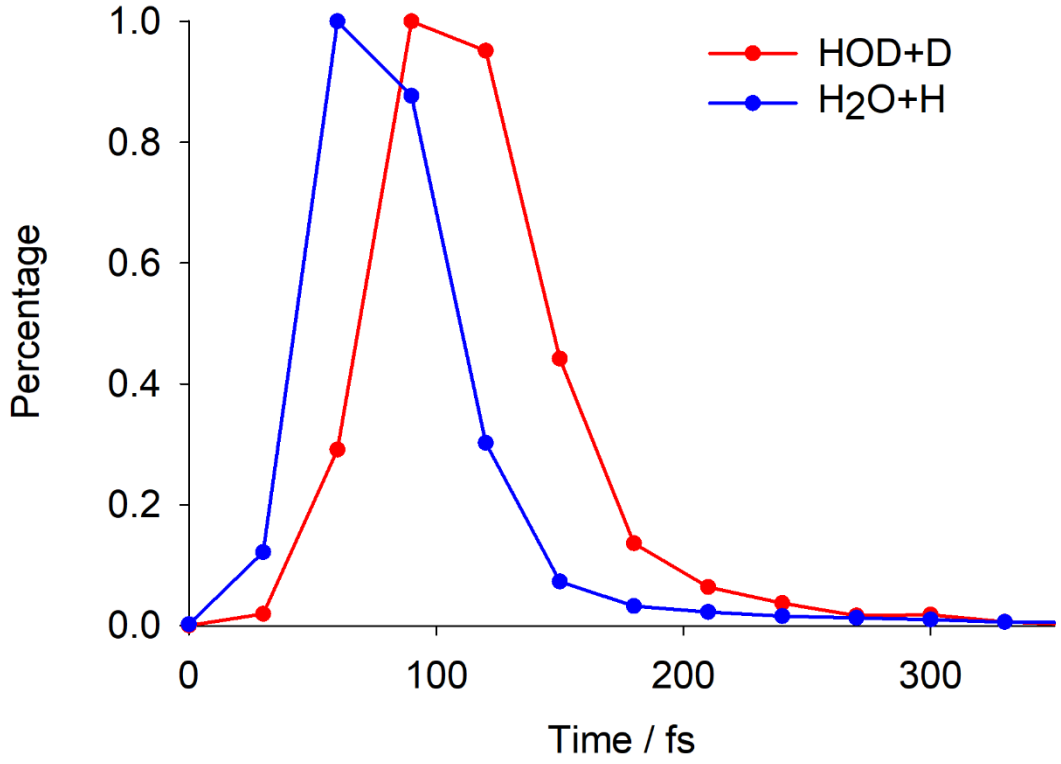

Figure 4. Calculated lifetime distributions of the trajectories for the H_2 + OH(A) → H_2O + H (blue line) and D_2 + OH(A) → HOD + D (red line) reactions.

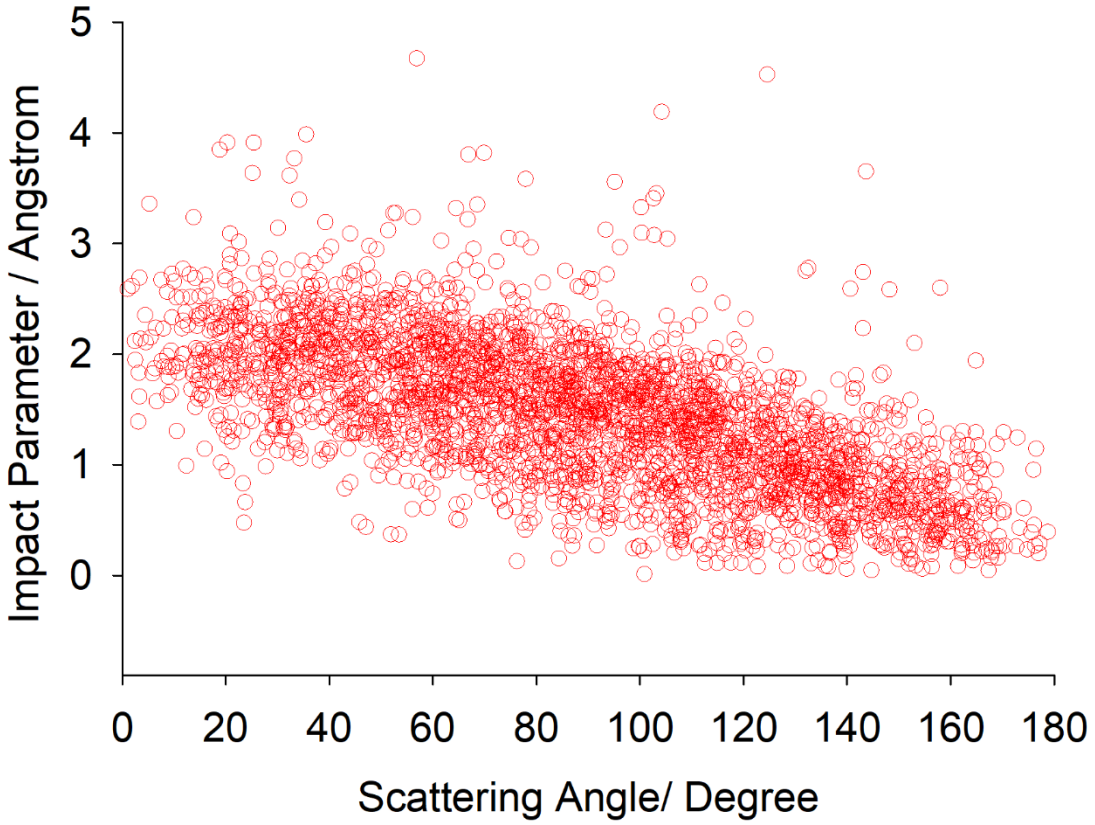

Figure 5. Correlation between the impact parameter and center of mass scattering angle for the D_2 + OH(A) → D+HOD reaction.

Figure 6 compares the calculated distribution of the relative kinetic energy of the HOD and D atom products from the OH(A) + D_2 → HOD + D reaction with the experimental[13] and previous theoretical results.[21] For a better comparison, all displayed distributions have been normalized to their highest peaks. The peak of our theoretical distribution is at 0.30 eV, which is in good agreement with the previous theoretical prediction.[21] These theoretical values are somewhat lower than the experimental peak of 0.6 eV.[13] While all distributions are peaked at relatively low kinetic energies, the theoretical widths appear to be slightly narrower than the

experimental one. These differences could have several possible origins, including the inevitable collisional energy spread in the crossed-beam experiment, the remaining inaccuracies in the DPEM, and the approximate nature of the dynamical method. In the same figure, the kinetic energy distribution for the OH(A) + H_2 → H_2O + H reaction at the same collision energy is shown. Like its deuterated counterpart, the distribution peaks at a low kinetic energy. These low kinetic energy distributions suggest that a large portion of the 4.8 eV energy release for this reactive channel is disposed into the internal degrees of freedom of the H_2O/HOD product.

It is interesting to note that both the calculated and measured kinetic energy distributions in Figure 6 have a single peak and decay to zero after 2 eV. While the OH(A) + D_2 → D_2O + H channel was not investigated in the molecular beam experiment,[13] the OH(A) + H_2 → H_2O + H distribution in the same figure has the qualitatively the same shape. This is different from the bimodal kinetic energy distribution reported by Lester and coworkers, where a weaker peak is also present at high kinetic energy (~2.6 eV) in addition to a high energy peak below 0.5 eV.[12] This secondary peak, which is more predominant for the OD + H_2 → H_2O + D reaction, was assigned to an insertion pathway. We have extensively searched for trajectories that follow to this pathway, but unfortunately very few (~0.01%) insertion trajectories were found in both the H_2 + OH and D_2 + OH cases. As pointed out in Ref. 22, the insertion pathway (shown in the lower panel of Figure 1) passes through the C_{2v} CI between the 3^1A and 2^1A states and the long-lived H_3O intermediate complex on the 2^1A state could provide multiple chances to cross the C_{2v} CI. However, a detailed

analysis of the DPEM identified a barrier for the formation of the H_3O intermediate that is 0.7 eV above the C_{2v} CI, as shown in Figure 1b, which prevented the formation of the H_3O intermediate. The small number of insertion trajectories were found to be direct process crossing the C_{2v} CI to the 1^2A state without formation of the H_3O intermediate complex on the 2^1A state. While there is a H_3O well on the 1^2A PES, the trajectories do not stay in the well long because the barrier to its decomposition is low. Hence, the extremely small proportion of insertion trajectories observed in our calculation can be rationalized by the preference of hopping near C_{2v} CI, which results in few C_{2v} CI crossings. For those C_{2v} nonadiabatic trajectories, some will end with the nonreactive quenching channel, further reducing the chance for the reactive quenching. Interestingly, the earlier simulations by Collins *et al*. also found little evidence for the insertion pathway.[21]

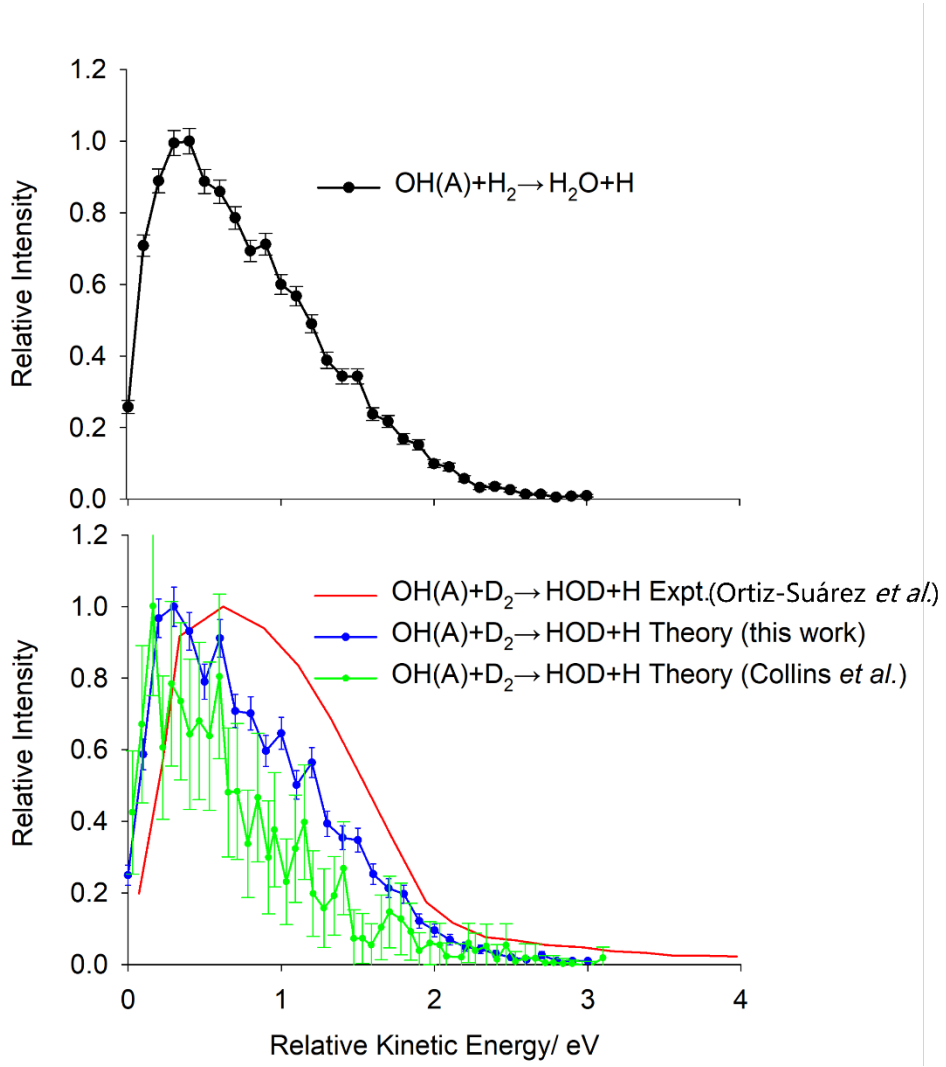

Figure 6. Product kinetic energy distributions for the H_2 + OH(A) → H_2O + H (upper panel) and D_2 + OH(A) → HOD+D (lower panel) reactions at a collision energy of 0.16 eV. The latter is compared with the experimental[13] and previous theoretical distributions.[21]

One might argue that the barrier is too high for trajectories to access the H_3O region at the collision energies. To test this assumption, we performed an additional calculation with collisional energy of 1.0 eV which is higher than the barrier. Although the total energy is now above the barrier, this attempt failed to significantly

increase the proportion of the insertion channel (0.02%). It appears that further improvement of the DPEM is needed for this region. Previous ab initio studies with larger MR-SDCI wave functions showed a barrier height of 700 cm^{-1},[22] much lower than the one in the MZGY DPEM. However, those studies were unable to describe the reactive quenching channel. The current DPEM is fit to ab initio that uses a smaller, but more flexible, MR-SDCI wave function, and the DPEM reflects this ab initio result. This suggests that there might still be room for improvement in the ab initio description.

Because of the availability of a detailed list of vibrational energy levels, we have used the 1GB method to obtain the vibrational distribution of the H_2O product in the OH(A) + H_2 → H_2O + H reaction. Figure 7 presents the classical rotational and vibrational energy distributions. It is clear from these figures that the energy disposal is almost exclusively in the vibrational excitation of the H_2O product. Populations of the vibrational states of $H_2O^{(v_{ss},v_b,v_{as})}$ obtained by 1GB is also shown in the right panel, which is in reasonable agreement with the classical vibrational energy distribution. It should be noted that the assigned vibrational states above 3.9 eV are incomplete as Ref. [42] did not assign all the vibrational states in this region. As a result, the 1GB distribution does not contain their populations in this range. Our rotational energy distribution is slightly cooler than the previous adiabatic QCT results by Fu *et al.*[20] while the vibrational energy distribution is somewhat hotter than that of Conte *et*

al.[24] This minor difference is presumably due to the assumption that all different CIs are equally approached in their QCT calculations, and/or differences in the PESs.

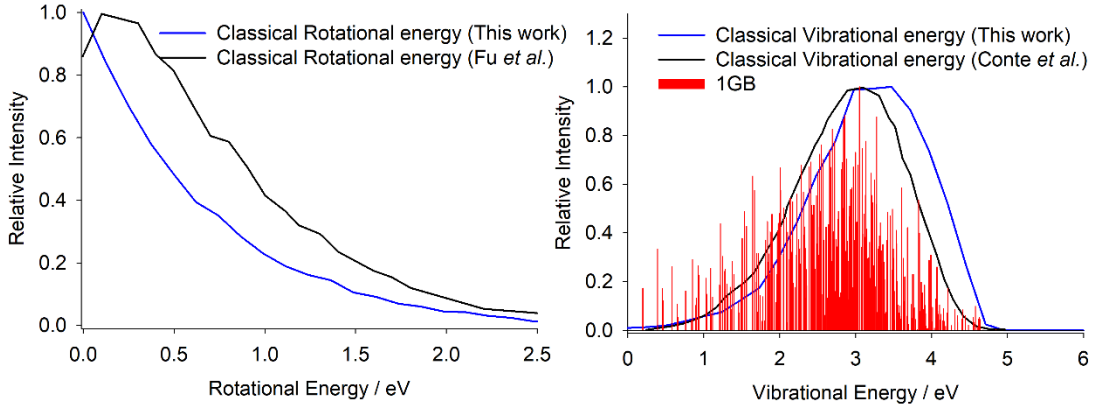

Figure 7. Calculated rotational energy distribution (left panel) and classical vibrational energy distribution (right panel) of H_2O formed from the H_2 + OH(A) → H + H_2O reaction at 0.16 eV. The classical rotational energy from QCT results by Fu *et al.* [20] and classical vibrational energy distribution by Conte *et al.*[24] are also shown for comparison. These two previous QCT studies were performed on the same adiabatic PES with the same total energy. The red vertical bars in the right panel represent populations of H_2O vibrational states as a function of vibrational energy.

This high vibrational excitation of the H_2O and cool translational excitation can be rationalized by the extended SVP model described in Section II. Figure 8 presents the *g* and *h* vectors at the minimum energy crossing of the linear 2^2A-3^2A CI seam. These vectors span the branching space in which the electronic degeneracy is lifted. Because of the cone-shape of the CI seam, it is not difficult to recognize that the main

forces acting on the system in the lower adiabat is along the *g* and *h* vectors after the nonadiabatic transition. Table I presents the SVP values for the vibrational and translational modes of the products in both the reactive and nonreactive quenching channels. For the nonreactive channel, the *g* and *h* vectors have moderate projections on the rotational and vibrational modes of both the OH and H_2 fragments, but the largest projection is on the translational mode by the *g* vector. This result is consistent with the previous quantum dynamics results in the non-reactive quenching channel,[31]

which showed moderate excitations in the internal modes of the two diatoms.

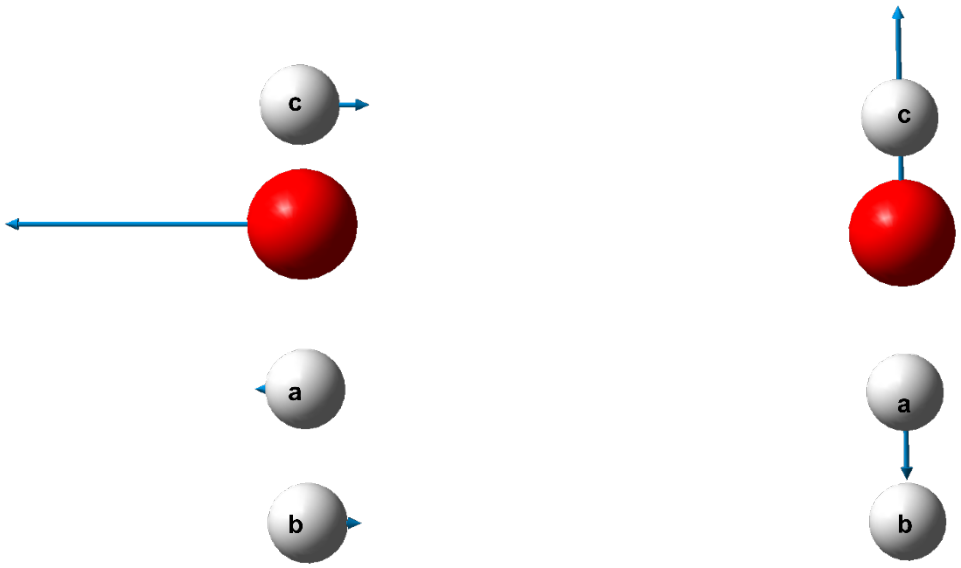

Figure 8. Mass-scaled $\sqrt{m_i}$ **g** (left) and **h** (right) vectors for the 2^2A-3^2A minimum energy crossing in collinear geometry. r_{OH_a}=1.197 Å, r_{OH_b} = 2.137 Å, r_{OH_c} = 0.963 Å, r_{OH_c} = 0.940 Å.

For the reactive quenching channel, both the *g* and *h* vectors have larger projections on the vibrational modes of the H_2O product than on the relative translational mode between H and H_2O. Specifically, the *g* vector has a large projection on the antisymmetric stretching (as) mode, while the *h* vector has a large projection on the bending (b) mode. For the symmetric stretching (ss) mode, both *g* and *h* vectors have moderate projections. This can be easily understood as the *g* vector is mostly along the antisymmetric stretching coordinate and the *h* vector lies along the bending coordinate, as shown in Figure 8. The symmetric stretching mode overlaps slightly with both *g* and *h* vector at the linear transition state.

Table I. For $OH(A^2\Sigma_g^+)+H_2(X^1\Sigma_g^+)\rightarrow H_2O(\tilde{X}^1A_1)+H$ reactive channel, projection of the vibrational, rotational, and translational modes onto the *g* and *h* vectors at the minimum energy crossing of linear CI. The geometry and corresponding *g* and *h* vectors are shown in Figure 8.

	g-vector	*h*-vector
$OH(A^2\Sigma_g^+)+H_2(X^1\Sigma_g^+)\rightarrow H_2O(\tilde{X}^1A_1)+H$		
$Q(\text{trans})$	0.097	0
$Q(\nu_{ss})$	0.22	0.23
$Q(\nu_b)$	0.14	0.26
$Q(\nu_{as})$	0.45	0.17
$OH(A^2\Sigma_g^+)+H_2(X^1\Sigma_g^+)\rightarrow OH(X^2\Pi)+H_2(X^1\Sigma_g^+)$		

$Q(\text{trans})$	0.48	0
$Q(R_{OH})$	0	0.42
$Q(R_{H_2})$	0	0.37
$Q(v_{OH})$	0.19	0
$Q(v_{H_2})$	0.32	0

Figure 9 presents the 1GB total vibrational distributions of each mode obtained by summation over other two modes, from which we can see the bending mode is more excited than other two vibrational modes. The average vibrational quantum number by 1GB and harmonic energy for each mode is v_b=7 and 1.48 eV for bending, v_s=2 and 1.14 eV for symmetric stretching, and v_a=2 and 1.09 eV for asymmetric stretching. These results show qualitative similarities as the earlier QCT study.[24] However, we note that the SVP model is not able to predict quantitatively the extent of product state distributions because of the post-bottleneck dynamics.

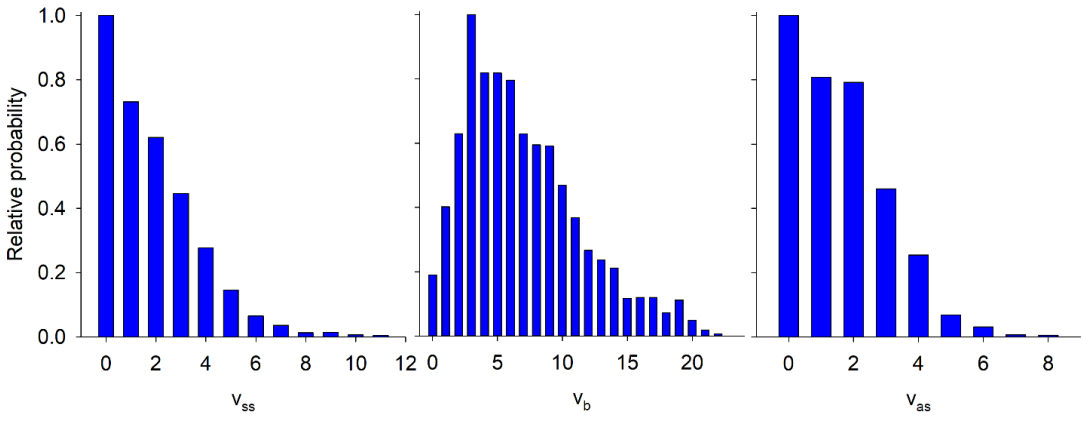

Figure 9. Total 1GB vibrational distributions of the three vibration modes of the H_2O product for the H_2 + OH(A) → H + H_2O reaction at 0.16 eV. v_{ss}, v_b, v_{as} denote symmetric stretching, bending, and asymmetric stretching modes, respectively.

IV. Conclusions

In this work, we perform semi-classical trajectory surface hopping calculations on the reactive quenching reaction, $OH\left(A^2\Sigma_g^+\right)$ + $H_2\left(X^1\Sigma_g^+\right)$ → $H_2O\left(\tilde{X}^1A_1\right)$ + H, using an accurate DPEM. It is shown that the reactive quenching shares the same nonadiabatic origin as the nonreactive quenching channel, and the nonadiabatic transitions occur mostly near the minimum energy crossing of the CIs near collinear HO-HH geometry. The calculated product translational energy and angular distributions are in reasonable agreement with the molecular beam experiment by Ortiz-Suárez *et al.*[13] and with previous theoretical calculations of Collins *et al.*[21] It is also shown that the H_2O/HOD vibrational modes, particularly the bending mode, are highly excited, which is also consistent with earlier theoretical understanding of the post-quenching dynamics on the ground electronic state PES.[20, 24] The vibrational excitation is rationalized by the Sudden Vector Projection model in which mode-specific product energy disposal is quantified by the projection of the product normal modes onto the *h* and *g* vectors of the relevant CI.

Despite these successes, our model did not find significant presence of the insertion mechanism identified by the earlier isotope experiments, despite the

existence of a pronounced H_3O well in the Rydberg region. Analysis of the DPEM revealed that this channel is hindered by a significant barrier, which prevented trajectories to enter the well. Our results are apparently consistent with an earlier theoretical study, which also failed to see much insertion dynamics. Further investigations of this issue, perhaps a refinement of the DPEM, are warranted.

Acknowledgements: This work was supported by the Department of Energy (DE-SC0015997 to H. G. and D. R. Y.). RC thanks Università degli Studi di Milano ("PSR, Azione A Linea 2 - Fondi Giovani Ricercatori") for support. The computation was performed at the Center for Advanced Research Computing (CARC) at UNM.

References:

(1) Gardiner, W. C. *Combustion Chemistry*; Springer, 1984.
(2) Wayne, R. P. *Chemistry of Atmospheres*; Oxford University Press, 2000.
(3) Crosley, D. R. Laser Probes for Combustion Chemistry. *ACS Symp. Ser.* **1980**, *134* 3-18.
(4) Crosley, D. R. Rotational and translation effects in collisions of electronically excited diatomic hydrides. *J. Phys. Chem.* **1989**, *93*, 6273-6282.
(5) Lehman, J. H.; Lester, M. I. Dynamical outcomes of quenching: Reflections on a conical intersection. *Annu. Rev. Phys. Chem.* **2014**, *65*, 537-555.
(6) Anderson, D. T.; Todd, M. W.; Lester, M. I. Reactive quenching of electronically excited OH radicals in collisions with molecular hydrogen. *J. Chem. Phys.* **1999**, *110*, 11117-11120.
(7) Todd, M. W.; Anderson, D. T.; Lester, M. I. Reactive quenching of OH A $^2\Sigma^+$ in collisions with molecular deuterium via nonadiabatic passage through a conical intersection. *J. Phys. Chem. A* **2001**, *105*, 10031-10036.
(8) Cleary, P. A.; Dempsey, L. P.; Murray, C.; Lester, M. I.; Kłos, J.; Alexander, M. H. Electronic quenching of OH $A^2\Sigma^+$ radicals in single collision events with molecular hydrogen: Quantum state distribution of the OH $X^2\Pi$ products. *J. Chem. Phys.* **2007**, *126*, 204316.
(9) Dempsey, L. P.; Murray, C.; Lester, M. I. Product branching between reactive and nonreactive pathways in the collisional quenching of OH $A^2\Sigma^+$ radicals by H_2. *J. Chem. Phys.* **2007**, *127*, 151101.
(10) Dempsey, L. P.; Murray, C.; Cleary, P. A.; Lester, M. I. Electronic quenching of OH $A^2\Sigma^+$ radicals in single collision events with H_2 and D_2: a comprehensive quantum state distribution of the OH $X^2\Pi$ products. *Phys. Chem. Chem. Phys.* **2008**, *10*, 1424-1432.
(11) Lehman, J. H.; Dempsey, L. P.; Lester, M. I.; Fu, B.; Kamarchik, E.; Bowman, J. M. Collisional quenching of OD $A^2\Sigma^+$ by H_2: Experimental and theoretical studies of the state-resolved OD $X^2\Pi$ product distribution and branching fraction. *J. Chem. Phys.* **2010**, *133*, 164307.
(12) Lehman, J. H.; Bertrand, J. L.; Stephenson, T. A.; Lester, M. I. Reactive quenching of OD $A^2\Sigma^+$ by H_2: Translational energy distributions for H- and D-atom product channels. *J. Chem. Phys.* **2011**, *135*, 144303.
(13) Ortiz-Suárez, M.; Witinski, M. F.; Davis, H. F. Reactive quenching of OH($A^2\Sigma^+$) by D_2 studied using crossed molecular beams. *J. Chem. Phys.* **2006**, *124*, 201106.
(14) Brouard, M.; Lawlor, J.; McCrudden, G.; Perkins, T.; Seamons, S. A.; Stevenson, P.; Chadwick, H.; Aoiz, F. J. An experimental study of OH($A^2\Sigma^+$) + H_2: Electronic quenching, rotational energy transfer, and collisional depolarization. *J. Chem. Phys.* **2017**, *146*, 244313.
(15) Lester, M. I.; Loomis, R. A.; Schwartz, R. L.; Walch, S. P. Electronic quenching of OH $A^2\Sigma^+$ (v' = 0, 1) in complexes with hydrogen and nitrogen. *J. Phys. Chem. A* **1997**, *101*, 9195-9206.

(16) Yarkony, D. R. Substituent effects and the noncrossing rule: The importance of reduced symmetry subspaces. I. The quenching of OH($A\ ^2\Sigma^+$) by H_2. *J. Chem. Phys.* **1999**, *111*, 6661-6664.
(17) Hoffman, B. C.; Yarkony, D. R. The role of conical intersections in the nonadiabatic quenching of OH($A^2\Sigma^+$) by molecular hydrogen. *J. Chem. Phys.* **2000**, *113*, 10091-10099.
(18) Zhang, P.-Y.; Lu, R.-F.; Chu, T.-S.; Han, K.-L. Quenching of OH($A^2\Sigma^+$) by H_2 through conical intersections: Highly excited products in nonreactive channel. *J. Phys. Chem. A* **2010**, *114*, 6565-6568.
(19) Zhang, P.-Y.; Lu, R.-F.; Chu, T.-S.; Han, K.-L. Nonadiabatic quantum reactive scattering of the OH($A^2\Sigma^+$)+D_2. *J. Chem. Phys.* **2010**, *133*, 174316.
(20) Fu, B.; Kamarchik, E.; Bowman, J. M. Quasiclassical trajectory study of the postquenching dynamics of OH $A^2\Sigma^+$ by H_2/D_2 on a global potential energy surface. *J. Chem. Phys.* **2010**, *133*, 164306.
(21) Collins, M. A.; Godsi, O.; Liu, S.; Zhang, D. H. An ab initio quasi-diabatic potential energy matrix for OH($^2\Sigma$) + H_2. *J. Chem. Phys.* **2011**, *135*, 234307.
(22) Dillon, J.; Yarkony, D. R. On the mechanism for the nonadiabatic reactive quenching of OH($A^2\Sigma^+$) by $H_2(^1\Sigma_g^+)$: The role of the 2^2A state. *J. Chem. Phys.* **2013**, *139*, 064314.
(23) Dillon, J.; Yarkony, D. R. Seams of conical intersections relevant to the quenching of OH($A^2\Sigma^+$) by collisions with H_2. *J. Phys. Chem. A* **2013**, *117*, 7344-7355.
(24) Conte, R.; Fu, B.; Kamarchik, E.; Bowman, J. M. A novel Gaussian binning (1GB) analysis of vibrational state distributions in highly excited H_2O from reactive quenching of OH* by H_2. *J. Chem. Phys.* **2013**, *139*, 044104.
(25) Shu, Y.; Kryven, J.; Sampaio de Oliveira-Filho, A. G.; Zhang, L.; Song, G.-L.; Li, S. L.; Meana-Pañeda, R.; Fu, B.; Bowman, J. M.; Truhlar, D. G. Direct diabatization and analytic representation of coupled potential energy surfaces and couplings for the reactive quenching of the excited $^2\Sigma^+$ state of OH by molecular hydrogen. *J. Chem. Phys.* **2019**, *151*, 104311.
(26) Malbon, C. L.; Zhao, B.; Guo, H.; Yarkony, D. R. On the nonadiabatic collisional quenching of OH(A) by H_2: a four coupled quasi-diabatic state description. *Phys. Chem. Chem. Phys.* **2020**, *22*, 13516-13527.
(27) Han, S.; de Oliveira-Filho, A. G. S.; Shu, Y.; Truhlar, D. G.; Guo, H. Semiclassical trajectory studies of reactive and nonreactive scattering of OH($A\ ^2\Sigma^+$) by H_2 based on an improved full-dimensional ab initio diabatic potential energy matrix. *ChemPhysChem* **2022**, *23*, e202200039.
(28) Yarkony, D. R. Diabolical conical intersections. *Rev. Mod. Phys.* **1996**, *68*, 985-1013.
(29) Yarkony, D. R. Nonadiabatic quantum chemistry - past, present and future. *Chem. Rev.* **2011**, *112*, 481-498.
(30) Domcke, W.; Yarkony, D. R. Role of conical intersections in molecular spectroscopy and photoinduced chemical dynamics. *Annu. Rev. Phys. Chem.* **2012**, *63*, 325-352.

(31) Zhao, B.; Han, S.; Malbon, C. L.; Manthe, U.; Yarkony, D. R.; Guo, H. Full-dimensional quantum stereodynamics of the non-adiabatic quenching of $OH(A^2\Sigma^+)$ by H_2. *Nat. Chem.* **2021**, *13*, 909-915.
(32) Bonnet, L. Classical dynamics of chemical reactions in a quantum spirit. *Int. Rev. Phys. Chem.* **2013**, *32*, 171-228.
(33) Czakó, G.; Bowman, J. M. Quasiclassical trajectory calculations of correlated product distributions for the $F+CHD_3(v_1 = 0,1)$ reactions using an ab initio potential energy surface. *J. Chem. Phys.* **2009**, *131*, 244302.
(34) Guo, H.; Jiang, B. The sudden vector projection model for reactivity: Mode specificity and bond selectivity made simple. *Acc. Chem. Res.* **2014**, *47*, 3679-3685.
(35) Jasper, A. W.; Truhlar, D. G. Non-Born-Oppenheimer molecular dynamics of Na···FH photodissociation. *J. Chem. Phys.* **2007**, *127*, 194306.
(36) *ANT (http://comp.chem.umn.edu/ant)*; University of Minnesota, Minneapolis: 2019. http://comp.chem.umn.edu/ant.
(37) Jasper, A. W.; Stechmann, S. N.; Truhlar, D. G. Fewest-switches with time uncertainty: A modified trajectory surface-hopping algorithm with better accuracy for classically forbidden electronic transitions. *J. Chem. Phys.* **2002**, *116*, 5424-5431.
(38) Tully, J. C. Molecular dynamics with electronic transitions. *J. Chem. Phys.* **1990**, *93*, 1061-1071.
(39) Eckart, C. Some studies concerning rotating axes and polyatomic molecules. *Phys. Rev.* **1935**, *47*, 552-558.
(40) Czako, G. Gaussian binning of the vibrational distributions for the $Cl + CH_4(v_{4/2}=0, 1) \rightarrow H + CH_3Cl(n_1n_2n_3n_4n_5n_6)$ reactions. *J. Phys. Chem. A* **2012**, *116*, 7467-7473.
(41) Truhlar, D. G.; Muckerman, J. T. Reactive scattering cross sections III: Quasiclassical and semiclassical methods. In *Atom-Molecule Collision Theory*, Bernstein, R. B. Ed.; Plenum, 1979; pp 505-566.
(42) Császár, A. G.; Mátyus, E.; Szidarovszky, T.; Lodi, L.; Zobov, N. F.; Shirin, S. V.; Polyansky, O. L.; Tennyson, J. First-principles prediction and partial characterization of the vibrational states of water up to dissociation. *J. Quant. Spectrosc. Radiat. Transf.* **2010**, *111*, 1043-1064.
(43) Jiang, B.; Guo, H. Relative efficacy of vibrational vs. translational excitation in promoting atom-diatom reactivity: Rigorous examination of Polanyi's rules and proposition of sudden vector projection (SVP) model. *J. Chem. Phys.* **2013**, *138*, 234104.
(44) Yarkony, D. R. On the adiabatic to diabatic states transformation near intersections of conical intersections. *J. Chem. Phys.* **2000**, *112*, 2111-2120.